

The physical chemistry of $[M(H_2O)_4(NO_3)_2]$ ($M = Mn^{2+}, Co^{2+}, Ni^{2+}, Cu^{2+}, Zn^{2+}$) complexes: computational studies of their structure, energetics and the topological properties of the electron density

Pradeep R. Varadwaj · Helder M. Marques

Received: 21 May 2010/Accepted: 2 July 2010/Published online: 17 July 2010
© Springer-Verlag 2010

Abstract The complexes of M^{2+} ($M = Mn, Co, Ni, Cu, Zn$), trans- $[M(H_2O)_4(NO_3)_2]$ in their high-spin ground electronic states have been investigated theoretically for the first time using several correlated DFT levels as well as with the MP2 method in conjunction with two different basis sets, 6-311++G(d, p) and LANL2TZ+/6-311++G(d, p), to examine their equilibrium structures and stabilities. Among the correlated methods, the X3LYP level together with the 6-311++G(d, p) basis set gives the best estimate of geometries in these complexes. The metal–ligand binding energies obtained follow the trend $Cu^{2+} > Ni^{2+} > Zn^{2+} > Co^{2+} > Mn^{2+}$ across the series examined, in precise agreement with the Irving–Williams series. The DFT methods largely overestimate the binding energies compared to the MP2 level and the trend follows the order PW91PW91 < PBEPBE < X3LYP < B3LYP < MP2. The use of an ECP basis on the central metal cation and a 6-311++G(d, p) basis set on the main group elements increases the binding energies of the complexes compared to that found using the full-core basis set 6-311++G(d, p) and the energy difference between

them can be as large as 20 kcal mol⁻¹. There are significant differences between the structures calculated in the gas phase and those calculated with the PCM model to simulate the effect of solvent. Solvation shortens the M–OH₂ bonds and lengthens the M–ONO₂ bonds such that the difference between the computed and the crystallographically observed bond lengths tends to decrease; it increases complex stability; and that it leads to the disappearance of two intramolecular H bonds between OH₂ and NO₃⁻ ligands that are present in the gas-phase structures. While there are differences between the natural populated atomic charges and Bader's approach of the quantum theory of atoms in molecules (QTAIM), all show charge transfer from the ligands to the metal ion. However, the MP2-level-computed charges were found to be unreliable compared with the DFT-derived charges. The metal–ligand bonding and the intramolecular H bonding in the complex are explored with QTAIM and the insight gained into the electronic structure of these complexes is discussed.

Keywords Late transition metal complexes · Nitrate complexes · Polarized continuum solvent model · Intramolecular hydrogen bonding · Atoms in molecules-DFT & MP2 studies

Electronic supplementary material The online version of this article (doi:10.1007/s00214-010-0781-z) contains supplementary material, which is available to authorized users.

P. R. Varadwaj (✉)
Faculty of Sciences, Department of Chemistry,
Okayama University, Tsushima-naka 3-1-1,
Okayama City, Okayama 700 8530, Japan
e-mail: pradeep@okayama-u.ac.jp

H. M. Marques
Molecular Sciences Institute, School of Chemistry,
University of the Witwatersrand, PO Wits,
Johannesburg 2050, South Africa
e-mail: holder.marques@wits.ac.za

1 Introduction

We have been studying the structure, the energetic stability and the nature of the bonding in several complexes of divalent metal ions from the first row using DFT methods [1–3]. Attention in those reports was focused on H₂O and NH₃ ligands, which are readily coordinated by these metal ions. In this work, we turn our attention to nitrate, a much weaker ligand for metal ions.

Nitrate is a versatile ligand, coordinating in a symmetrical bidentate fashion (as for example, in its coordination to Cd(II) in a polymeric structure in which metal ions are bridged by pyrazine to La³⁺ in La(NO₃)₆³⁻ [4]), in an unsymmetrical bidentate manner (as in its coordination to Ag(I) in a diphenylarsine complex of the metal [5]) and in unidentate fashion as in [Co(H₂O)₄(NO₃)₂] [6] and in [Ni(H₂O)₄(NO₃)₂] [7]. In the gas phase, it forms complexes of the type M(NO₃)₃ (M = Mg²⁺, Ca²⁺, Sr²⁺ and Ba²⁺) as determined from IR multi-photon dissociation spectroscopy [8]; DFT calculations (B3LYP/3-21G*) suggest bidentate coordination of the anion to the metal. Recently, a study at the DFT-B3LYP level in conjunction of a wide range of basis sets ranging from STO-3G to 6-311 + G* on the structural and vibrational properties of vanadyl nitrate, VO(NO₃)₃, was reported [9]. They found a structure where NO₃⁻ ligands are bidentate toward the metal while the third is monodentate. It was found that B3LYP/6-311G* and B3LYP/6-311++G* best reproduce the experimental (gas-phase electron diffraction) bond lengths of the complex with r.m.s.d. of 0.041 Å for bond lengths and 4.11° for valence angles.

In aqueous solution, NO₃⁻ is a poor ligand for metal ions; log *K* values for formation of the Mⁿ⁺-NO₃⁻ complex from the hexaaqua ions are -0.7 for Mn(II) [10], -0.15 for Co(II) [11], 0.08 for Ni(II) [11], -0.17 for Cu(II) [12] and -0.13 for Zn(II) [12]. Hence, nitrate salts are often used as supporting electrolytes in the potentiometric determination of stability constants [13].

The hydration of NO₃⁻ is not particularly strong [14], and a variety of diffraction methods suggest that between six and nine H₂O molecules interact with ion. Theoretical studies have been performed to elucidate the nature of the hydrated nitrate ion in clusters of the form [NO₃·nH₂O]⁻ (*n* = 1–8) [15–17]. The ion has a highly symmetrical solvation shell with three water molecules bound to it in a bidentate fashion, and there is extensive hydrogen bonding to the additional waters in the second hydration sphere.

We report here a DFT study using both B3LYP and X3LYP with 6-311++G(d, p) and LANL2TZ+ (on the metal)/6-311++G(d,p)(on other atoms) basis sets to examine the equilibrium structures, and energetic stabilities of complexes of the type [M(H₂O)₄(NO₃)₂] (M = Mn²⁺, Co²⁺, Ni²⁺, Cu²⁺, Zn²⁺). There are a number of reports of solid-state complexes of [M(H₂O)₄(NO₃)₂] where M = Mn²⁺ [6, 7, 18, 19], Co²⁺ [6, 7, 20, 21], Ni²⁺ [6, 7, 21–27] and Zn²⁺ [7, 28–30].

Since DFT hybrid functionals containing various amounts of HF exchange have been demonstrated to be more accurate than non-hybrid functionals for predicting a variety of physical properties of complexes of the type reported here [31], we have carried out the calculations with the widely used functionals B3LYP (20% HF) and

X3LYP (21.8% HF); the latter [32–34] is an extension of the former [35, 36], and handles weak interactions more satisfactorily. For reasons to be discussed later, we also performed the calculations using the GGA functionals PBEPBE [37] and PW91PW91 [38] and at the MP2 [39] level of theory. To explore the effect of a condensed phase on these structures, we repeated the calculations in a polarized continuum medium (PCM) [40, 41]. We compared the structural parameters from the energy-minimized structures with the available crystallographic information. Natural population analysis was carried out to assess the metal-to-ligand charge transfer effects in these complexes. We have continued our exploration [1–3] of the nature of metal-ligand bonding in transition metal complexes with mixed ligands using Bader's quantum theory of atoms in molecules (QTAIM) [42] to examine the topological properties of the electron density both in the structures obtained in the gas phase and those incorporating a solvation model.

2 Computational details

For each of the complexes of M²⁺, the optimized gas-phase geometries were obtained using GAUSSIAN 03 [43], and visualization was done with the help of the GAUSSVIEW 04 suite of programs [44]. All the complexes were energy-minimized under C_i symmetry (many of these complexes have this symmetry in the solid state) with the X3LYP [32–34] and B3LYP [35, 36] functionals utilizing unrestricted spins for Mn²⁺ (*S* = 5/2), Co²⁺ (*S* = 3/2), Ni²⁺ (*S* = 1), Cu²⁺ (*S* = 1/2) and restricted spin for Zn²⁺ (*S* = 0).

Two different basis sets were used in the calculations: (a) a full-core basis set of triple valence quality 6-311++G(d, p) augmented with p and d-polarization functions, and (b) a newly reported [45] triple zeta quality effective core potential (ECP) basis set LANL2TZ+ augmented with diffuse extension '+' centered on the metal and a full-core basis 6-311++G(d, p) on all other elements. The LANL2TZ+ basis set has been recommended for DFT calculations on transition metal complexes [45]; it consists of the original Hay-Wadt primitives contracted [5s5p3d] for the first row transition series. We chose to use two correlated functionals and two different basis sets to investigate their performance in calculating various properties of these complexes. In our experience [1–3], 6-311++G(d, p) is adequate for studies on transition metal complexes and was found to describe the molecular and electronic structural features of the complexes in a well-defined manner. For reasons to be discussed latter, we have extended our calculations in the gas phase at PBEPBE, PW91PW91, and MP2 levels with the same basis set.

Normal mode frequency calculations were performed analytically from the second derivatives of the B3LYP and

X3LYP potential energy surfaces with respect to the atom-fixed nuclear coordinates to determine whether each of the minimized structures corresponded to genuine stationary points. The convergence criterion with SCF = Fermi and ultrafine integration grid was stipulated in these calculations. Similar to our previous experiences with the Ni^{2+} and Co^{2+} complexes [1–3], we encountered SCF convergence failures when restricting the symmetry to the C_{2h} point group; either the calculations terminated without convergence or the structures produced were saddle point structures as evidenced by the presence of imaginary frequencies even though the geometry was virtually identical to that of the energy minimized structures obtained under C_i ; we have not reported on these structures here. The SCF convergence problem is not unexpected since transition metal ions have near-degenerate ground terms. Even under C_i , convergence failed quite often; small changes in the starting geometry eventually led to structures corresponding to the genuine local minimum energy configurations (IMAG = 0) reported in this work.

The stabilization energy (or binding energy) E_b , without zero-point vibration corrections, and the dissociation energy, E_d^c , incorporating the zero-point vibration energy correction, were calculated using Eqs. 1 and 2, where it is understood that all species are in the gas phase. In these equations, E is the total energy at 0 K, and ZPVCE is the zero-point vibrational corrected total energy. The total energy of the metal ions M^{2+} was evaluated for the high-spin states using single-point energy calculations using tight convergence and an ultrafine integration grid. The uncorrected energies, E_b , were finally corrected for the basis set superposition error using the counterpoise procedure of Boys and Bernardi [46].

These gas-phase structures were then re-optimized using the polarized continuum model (PCM) [40, 41] with water as a solvent and UAKS atomic radii with TSNUM = 100, and TSARE = 0.3.

$$E_b([M(\text{NO}_3)_2(\text{H}_2\text{O})_4]) = E([M(\text{NO}_3)_2(\text{H}_2\text{O})_4]) - [E(M)^{2+} + 2E(\text{NO}_3^-) + 4E(\text{H}_2\text{O})] \quad (1)$$

$$E_d^c([M(\text{NO}_3)_2(\text{H}_2\text{O})_4]) = [E(M)^{2+} + 2\text{ZPVCE}(\text{NO}_3^-) + 4\text{ZPVCE}(\text{H}_2\text{O})] - \text{ZPVCE}([M(\text{NO}_3)_2(\text{H}_2\text{O})_4]) \quad (2)$$

The atom-centered partial charges were calculated on the optimized structures within the framework of natural population analysis (NPA) method [47] using natural bond orbital (NBO) 3.1 [48, 49] as implemented in GAUSSIAN 03 for both the α - and β -sets of MOs for the open shell systems. Based on this approach, the natural population $q_i^{(A)}$ of orbital $\varphi_i^{(A)}$ on atom A is the diagonal density matrix element in the natural atomic orbital (NAO) basis, which may be summed to give the total

number of electrons and the natural charge $Q^{(A)}$ on atom A with atomic number $Z^{(A)}$. The ligand-to-metal charge transfer (ΔQ) was calculated as a difference of the formal +2 charge of the metal ion and the charge determined upon the complex formation.

Since as well as the inter-ligand interactions in these complexes is presumably a donor–acceptor delocalization, we performed NBO natural localized molecular orbital (NLMO) analysis to evaluate the second-order perturbative energy $\Delta E^{(2)}$ caused by charge-transfer interactions.

The topological properties of the charge density in the complexes were analyzed with QTAIM using the AIMALL program [50]. The charge density (ρ_c), its Laplacian ($\nabla^2 \rho_c$), the ellipticity (ε) and the total energy density (H_c) allow for classification of the nature of a bond critical point (BCP).

3 Results and discussion

3.1 Structure

The starting structure for energy minimization was, where available, a representative solid-state structure. While structures of both cis- and trans-[M(H₂O)₄(NO₃)₂] complexes are available for at least some of the later first row metals, there are more of the latter and we confined our calculations to these isomers. Figure 1 shows, as example, the crystal structure of trans-[Mn(H₂O)₄(NO₃)₂] [6] and the energy minimized B3LYP/6-311++G(d, p) structure. In Table 1, the bond lengths obtained at the various levels of theory and the mean crystallographic bond lengths are

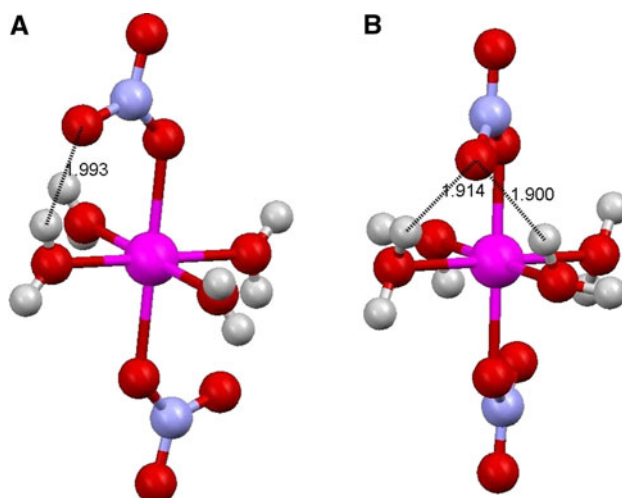


Fig. 1 **a** The solid-state structure and **b** the B3LYP/6-311++G(d, p) structure (in the gas phase) of trans-[Mn(H₂O)₄(NO₃)₂]. Hydrogen bonds between coordinated NO₃[−] and H₂O are shown (distances in Å)

Table 1 A comparison between bond lengths in trans-[M(H₂O)₄(NO₃)₂] complexes found crystallographically and calculated by a variety of theoretical methods

Complex	Functional	Basis set	Phase	M-OH ₂ /Å	σ	Δ^a	M-ONO ₂ /Å	σ	Δ^a	O-NO ₂ /Å	σ	Δ^a	N-NO ₂ /Å	σ	Δ^a
[Mn(H₂O)₄(NO₃)₂] X-ray structures [6, 7]															
	B3LYP	6-311++G(d, p)	Gas	2.131	0.002	2.243	0.001	1.257	0.005	1.229	0.009				
	B3LYP	LANL2TZ//6-311++G(d, p)	Gas	2.246	0.004	-0.115	2.149	0.000	0.094	1.291	0.000	-0.034	1.243	0.038	-0.014
	B3LYP	6-311++G(d, p)	Gas	2.247	0.003	-0.117	2.155	0.000	0.087	1.291	0.000	-0.034	1.243	0.038	-0.014
	X3LYP	6-311++G(d, p)	Gas	2.239	0.004	-0.109	2.148	0.000	0.094	1.289	0.000	-0.032	1.242	0.038	-0.013
	X3LYP	LANL2TZ//6-311++G(d, p)	Gas	2.242	0.002	-0.111	2.154	0.000	0.089	1.289	0.000	-0.032	1.242	0.038	-0.013
	PBEPBE	6-311++G(d, p)	Gas	2.247	0.005	-0.117	2.146	0.000	0.097	1.303	0.000	-0.046	1.256	0.043	-0.027
	PW91PW91	6-311++G(d, p)	Gas	2.240	0.005	-0.109	2.143	0.000	0.100	1.302	0.000	-0.046	1.256	0.043	-0.027
	MP2	6-311++G(d, p)	Gas	2.235	0.003	-0.105	2.152	0.000	0.090	1.288	0.000	-0.032	1.247	0.030	-0.018
	B3LYP	Solvent ^b	2.202	0.025	-0.071	2.207	0.000	0.035	1.279	0.000	-0.022	1.244	0.013	-0.015	
	X3LYP	Solvent ^b	2.201	0.021	-0.071	2.196	0.000	0.047	1.278	0.000	-0.021	1.242	0.013	-0.013	
[Co(H₂O)₄(NO₃)₂] X-ray structures [6, 7, 20, 21, 78]															
	B3LYP	6-311++G(d, p)	Gas	2.151	0.032	2.067 ^c	0.059	0.000	0.088	1.298	0.000	-0.060	1.241	0.036	0.025
	B3LYP	LANL2TZ//6-311++G(d, p)	Gas	2.157	0.003	-0.099	2.067	0.000	0.080	1.297	0.000	-0.059	1.241	0.038	0.025
	X3LYP	6-311++G(d, p)	Gas	2.157	0.003	-0.094	2.058	0.000	0.089	1.295	0.000	-0.057	1.239	0.036	0.027
	X3LYP	LANL2TZ//6-311++G(d, p)	Gas	2.146	0.003	-0.094	2.065	0.000	0.082	1.294	0.000	-0.056	1.239	0.038	0.027
	X3LYP	LANL2TZ//6-311++G(d, p)	Gas	2.152	0.003	-0.094	2.048	0.000	0.099	1.313	0.000	-0.075	1.252	0.039	0.014
	PBEPBE	6-311++G(d, p)	Gas	2.148	0.010	-0.102	2.151	0.009	-0.095	2.044	0.000	0.104	1.312	0.000	-0.074
	PW91PW91	6-311++G(d, p)	Gas	2.165	0.000	-0.080	2.136	0.000	0.095	2.052	0.000	0.095	1.293	0.000	-0.055
	MP2	6-311++G(d, p)	Gas	2.142	0.000	-0.050	2.130	0.000	0.017	1.281	0.000	-0.043	1.244	0.013	0.022
	B3LYP	Solvent ^b	2.107	0.001	-0.047	2.128	0.000	0.019	1.279	0.000	-0.041	1.242	0.013	0.024	
	X3LYP	Solvent ^b	2.101	0.001	-0.047	2.103	0.046	0.030	2.080	0.020	0.133	1.234	0.013	1.279	0.007
[Ni(H₂O)₄(NO₃)₂] X-ray structures [6, 7, 27]															
	B3LYP	6-311++G(d, p)	Gas	2.104	0.005	-0.058	2.050	0.000	0.030	1.294	0.000	-0.060	1.242	0.037	0.037
	B3LYP	LANL2TZ//6-311++G(d, p)	Gas	2.104	0.005	-0.058	2.054	0.000	0.026	1.293	0.000	-0.059	1.242	0.038	0.037
	X3LYP	6-311++G(d, p)	Gas	2.099	0.007	-0.053	2.047	0.000	0.033	1.292	0.000	-0.058	1.241	0.037	0.039
	X3LYP	LANL2TZ//6-311++G(d, p)	Gas	2.100	0.005	-0.054	2.051	0.000	0.029	1.291	0.000	-0.057	1.241	0.038	0.039
	PBEPBE	6-311++G(d, p)	Gas	2.106	0.005	-0.060	2.052	0.000	0.028	1.306	0.000	-0.072	1.254	0.041	0.025
	PW91PW91	6-311++G(d, p)	Gas	2.100	0.004	-0.054	2.048	0.000	0.032	1.305	0.000	-0.071	1.254	0.042	0.025
	MP2	6-311++G(d, p)	Gas	2.085	0.008	-0.039	2.027	0.000	0.053	1.292	0.000	-0.058	1.245	0.029	0.035
	B3LYP	Solvent ^b	2.104	0.006	-0.058	2.050	0.000	0.030	1.294	0.000	-0.060	1.242	0.037	0.037	
	X3LYP	Solvent ^b	2.084	0.018	-0.038	2.079	0.000	0.002	1.283	0.000	-0.049	1.241	0.013	0.039	

Table 1 continued

Complex	Functional	Basis set	Phase	$M-OH_2/\text{\AA}$	σ	Δ^a	$M-ONO_2/\text{\AA}$	σ	Δ^a	$O-NO_2/\text{\AA}$	σ	Δ^a	$N-NO_2/\text{\AA}$	σ	Δ^a
$[\text{Cu}(\text{H}_2\text{O})_4(\text{NO}_3)_2]$ X-ray structures ^c															
	B3LYP	6-311++G(d, p)	Gas	2.046		1.976	0.000	1.306	0.000	1.235	0.029				
	B3LYP	LANL2TZ+/-6-311++G(d, p)	Gas	2.424		1.979	0.000	1.305	0.000	1.235	0.030				
	X3LYP	6-311++G(d, p)	Gas	2.069	2.357	1.973	0.000	1.304	0.000	1.234	0.030				
	X3LYP	LANL2TZ+/-6-311++G(d, p)	Gas	2.043	2.405	1.977	0.000	1.303	0.000	1.234	0.030				
	PBEPBE	6-311++G(d, p)	Gas	2.087	2.345	1.995	0.000	1.316	0.000	1.246	0.029				
	PW91PW91	6-311++G(d, p)	Gas	2.067	2.067	1.991	0.000	1.316	0.000	1.246	0.030				
	MP2	6-311++G(d, p)	Gas	2.446	2.061	2.429	2.034	1.952	0.000	1.303	0.000	1.239	0.022		
	B3LYP	6-311++G(d, p)	Solvent ^b	2.314	2.001	2.358	2.002	2.037	0.000	1.290	0.000	1.239	0.013		
	X3LYP	6-311++G(d, p)	Solvent ^b	2.351	2.002	2.030	0.000	1.289	0.000	1.237	0.013				
$[\text{Zn}(\text{H}_2\text{O})_4(\text{NO}_3)_2]$ X-ray structures [7]															
	B3LYP	6-311++G(d, p)	Gas	2.121	0.051	-0.082	2.164	0.012	0.029	1.294	0.000	-0.026	1.242	0.037	-0.006
	B3LYP	6-311++G(d, p) (C_{2h})	Gas	2.113	0.058	-0.074	2.163	0.000	0.030	1.298	0.000	-0.030	1.240	0.034	-0.004
	B3LYP	LANL2TZ+/-6-311++G(d, p)	Gas	2.143	0.042	-0.104	2.166	0.000	0.027	1.291	0.000	-0.023	1.243	0.038	-0.007
	B3LYP	LANL2TZ+/-6-311++G(d, p) (C_{2h})	Gas	2.133	0.043	-0.094	2.170	0.000	0.023	1.294	0.000	-0.026	1.241	0.035	-0.005
	X3LYP	6-311++G(d, p)	Gas	2.116	0.048	-0.078	2.157	0.014	0.036	1.292	0.000	-0.024	1.240	0.037	-0.004
	X3LYP	LANL2TZ+/-6-311++G(d, p)	Gas	2.135	0.037	-0.097	2.167	0.010	0.026	1.289	0.000	-0.021	1.242	0.038	-0.006
	PBEPBE	6-311++G(d, p)	Gas	2.166	0.009	-0.127	2.095	0.000	0.098	1.305	0.000	-0.037	1.255	0.042	-0.019
	PW91PW91	6-311++G(d, p)	Gas	2.158	0.008	-0.120	2.092	0.000	0.101	1.304	0.000	-0.036	1.255	0.043	-0.019
	MP2	6-311++G(d, p)	Gas	2.088	0.047	-0.049	2.150	0.000	0.043	1.293	0.000	-0.025	1.245	0.028	-0.008
	B3LYP	6-311++G(d, p)	Solvent	2.121	0.021	-0.083	2.149	0.000	0.045	1.282	0.000	-0.014	1.243	0.013	-0.007
	X3LYP	6-311++G(d, p)	Solvent	2.128	0.018	-0.089	2.121	0.028	0.072	1.281	0.000	-0.013	1.241	0.013	-0.005

^a (Crystallographically observed)—(DFT-predicted)^b Polarized continuum model with water as a solvent and UAKS atomic radii^c A small Jahn–Teller distortion is evident in all five solid-state structure with two Co–OH₂ longer than the other two^d The average Co–OH₂ bond length has been used for these statistics^e There appear to be no structures of the type $[\text{Cu}(\text{H}_2\text{O})_4(\text{NO}_3)_2]$ reported. Because of Jahn–Teller distortion, two very different Cu–OH₂ bond lengths are observed

compared. All structures reported are genuine local minima.

Superficially, the gas-phase structures calculated by DFT methods are similar to the solid-state structures. The metal is six coordinate, each nitrate ligand binds in a monodentate manner and there is usually hydrogen bonding between an O of NO_3^- and a coordinated H_2O molecule. However, an examination of the values in Table 1 shows that invariably in the calculated structures the M–OH₂ bond is longer than the M–ONO₂ bond, whereas in all cases in the solid state the converse is true, as expected given that NO_3^- is a rather poor ligand for metal ions (vide supra). The calculations we have performed, using both GGA and hybrid functionals, both in the gas phase and in solvent, as well as MP2 calculations in the gas phase, overestimate the ligand-binding power of the NO_3^- ligand and, consequently, produce M–ONO₂ bonds that are too short (by up to 0.10 Å) and, conversely, M–OH₂ bonds that are too long (by between 0.04 and 0.13 Å). The O–NO₂ bond lengths are overestimated by about 0.04 Å on average, while the N–O bond lengths to the uncoordinated O atoms of NO_3^- are on average reproduced to better than 0.01 Å.

Despite this generally disappointing performance of these computational methods with complexes featuring a weakly coordinating ligand, we note that first, for a given point group symmetry, the mean M–OH₂ bond lengths are shorter (and hence closer to the crystallographically observed values) by about 0.01 Å when calculated using the 6-311++G(d, p) basis set with the X3LYP functional compared to the B3LYP functional, whereas both functionals give virtually identical M–ONO₂ bond lengths. Second, replacing the full-core basis set with an ECP LANL2TZ+ basis set on the metal ion has no significant effect on the M–OH₂ bond lengths for the Mn²⁺, Co²⁺ and Ni²⁺ complexes (with either B3LYP or X3LYP); Cu–OH₂ bond lengths increase by about 0.02 Å, whereas Zn²⁺–OH₂ bond lengths decrease by the same amount. The latter are now within 0.05 Å of the crystallographic values; this has to be treated with circumspection, however, given that there is only one single structure [7] of trans-[Zn(H₂O)₄(NO₃)₂] known. We conclude that use of X3LYP together with a 6-311++G(d, p) basis set gives the best estimate of the geometry in these complexes.

The expected Jahn–Teller distortion of the Cu²⁺ complex is observed; two Cu–OH₂ bonds are marginally longer (in the gas-phase structures) or marginally shorter (in the condensed phase structures) than the Cu–ONO₂ bonds, while the other two Cu–OH₂ bonds are very much longer (Table 1).

High-spin d⁷ Co²⁺ complexes should also undergo a (small) Jahn–Teller distortion. This is indeed observed in the solid-state structures, where the five known

[Co(H₂O)₄(NO₃)₂] complexes have a pair of longer and a pair of shorter Co–OH₂ bonds (2.043(15) and 2.067(32) Å, respectively). As can be seen from Table 1, two slightly different Co–OH₂ bond lengths are found; the differences between the two sets is very small if MP2 or a hybrid functional is used, but somewhat more pronounced in the case of calculations with a pure GGA functional. However, it is by no means certain that these small differences in bond length are in fact due to a Jahn–Teller distortion. Thus, one would expect the four metal–OH₂ bond lengths in each of the high-spin Mn²⁺ and Ni²⁺, and d¹⁰ Zn²⁺ complexes, to be identical. This is the case for the Mn²⁺ complexes in the gas phase, but inclusion of solvent leads to a very marked asymmetry. A comparison of the two structures (Figure S1 of the Supplementary Information) shows that in the gas-phase structure two neighboring H₂O molecules are each hydrogen-bonded to a coordinated NO_2^- ion. The difference between the Mn–OH₂ bonds is a mere 0.006 Å. In the solvent structure, only one (shorter) hydrogen bond persists; the Mn–OH₂ bond length to the H₂O involved in hydrogen bonding is now 0.036 Å shorter, presumably driven by the formation of the S(1,1)(6) motif.

In the case of trans-[Zn(NH₃)₄(NO₃)₂], we optimized the structure under both C_i symmetry and C_{2h} symmetry. Changing the symmetry from C_i to C_{2h} using B3LYP/6-311++G(d, p) has a very small effect on the geometry of the complex and a minor effect on complex stability (vide infra).

In addition to metal–ligand bonding, hydrogen bonds are formed between NO_3^- and the nearest neighboring H atoms of coordinated H₂O in the complexes (Fig. 1). There are four such bonds in each complex, two longer and two shorter, ranging from 1.840 to 2.151 Å in length, irrespective of the calculation method used. These interactions fulfill the geometric criteria to be considered as hydrogen bonds [$\angle \text{O}–\text{H}–\text{O}$ 138–143°, lengths < sum of the van der Waals radii of the O (1.52 Å) and H atoms (1.20 Å)]. To further characterize these bonds, we performed NBO NLMO and QTAIM studies discussed below.

3.2 Energetics

Irrespective of the level of theory utilized, the order of stability of complex formation is Cu²⁺ > Ni²⁺ > Zn²⁺ > Co²⁺ > Mn²⁺, in precise agreement with the Irving–Williams series (Table 2, Figure S2). Confining the symmetry of [Zn(H₂O)₄(NO₃)₂] to C_{2h} rather than C_i has minimal effect on the geometry of the complex, while the stability decreases by a mere 1.2 kcal mol⁻¹. Thus, changes in symmetry are not expected to affect the general conclusions reached in this work and we will confine attention to the C_i complexes.

Table 2 The energetic properties of the complexes

Complex	Method/basis	E_b	ZPE	E_d^c	BSSE	$(E_b\text{-BSSE})$
[Mn(H ₂ O) ₄ (NO ₃) ₂]	B3LYP/6-311++G(d,p)	-589.2	82.6	577.8	7.8	-581.4
	B3LYP/LANL2TZ+/6-311++G(d, p)	-592.2	82.5	580.8	7.7	-584.4
	X3LYP/6-311++G(d, p)	-594.6	82.8	582.6	8.0	-586.2
	X3LYP/LANL2TZ+/6-311++G(d, p)	-597.0	82.8	585.6	7.8	-589.2
	PBEPBE/6-311++G(d, p)	-602.4	80.1	591.6	9.2	-594.0
	PW91PW91/6-311++G(d, p)	-607.2	80.1	595.8	8.7	-598.2
	MP2/6-311++G(d, p)	-587.4			24.7	-562.8
[Co(H ₂ O) ₄ (NO ₃) ₂]	B3LYP/6-311++G(d, p)	-631.2	83.8	618.0	8.4	-622.8
	B3LYP/LANL2TZ+/6-311++G(d, p)	-643.2	84.0	630.0	19.1	-624.6
	X3LYP/6-311++G(d, p)	-636.0	84.1	622.8	6.8	-629.4
	X3LYP/LANL2TZ+/6-311++G(d, p)	-648.6	84.2	635.4	19.3	-629.4
	PBEPBE/6-311++G(d, p)	-652.8	81.1	640.2	7.5	-645.0
	PW91PW91/6-311++G(d, p)	-657.0	81.2	645.0	8.0	-649.2
	MP2/6-311++G(d, p)	-627.6			26.5	-601.2
[Ni(H ₂ O) ₄ (NO ₃) ₂]	B3LYP/6-311++G(d, p)	-652.2	84.6	638.4	8.5	-643.8
	B3LYP/LANL2TZ+/6-311++G(d, p)	-656.4	84.8	642.0	15.4	-640.8
	X3LYP/6-311++G(d, p)	-657.0	84.8	643.2	8.6	-648.0
	X3LYP/LANL2TZ+/6-311++G(d, p)	-661.2	85.1	647.4	15.5	-645.6
	PBEPBE/6-311++G(d, p)	-676.8	81.9	663.6	9.5	-667.2
	PW91PW91/6-311++G(d, p)	-681.6	82.0	668.4	10.0	-672.0
	MP2/6-311++G(d, p)	-648.0			28.9	-619.2
[Cu(H ₂ O) ₄ (NO ₃) ₂]	B3LYP/6-311++G(d, p)	-657.0	83.0	644.4	8.2	-648.6
	B3LYP/LANL2TZ+/6-311++G(d, p)	-659.4	83.2	646.8	13.7	-645.6
	X3LYP/6-311++G(d, p)	-660.6	83.3	648.0	7.9	-652.8
	X3LYP/LANL2TZ+/6-311++G(d, p)	-663.0	83.5	650.4	14.2	-648.6
	PBEPBE/6-311++G(d, p)	-685.8	80.0	674.4	8.7	-677.4
	PW91PW91/6-311++G(d, p)	-688.2	80.1	677.4	9.4	-679.2
	MP2/6-311++G(d, p)	-649.8			27.7	-622.2
[Zn(H ₂ O) ₄ (NO ₃) ₂]	B3LYP/6-311++G(d, p) (C _i)	-634.8	83.6	621.6	8.2	-626.4
	B3LYP/LANL2TZ+/6-311++G(d, p) (C _i)	-617.4	83.5	604.8	8.5	-609.0
	B3LYP/6-311++G(d, p) (C _{2h})	-633.6	82.9	621.0	8.3	-625.2
	B3LYP/LANL2TZ+/6-311++G(d, p) (C _{2h})	-616.2	82.9	604.2	8.6	-607.8
	X3LYP/6-311++G(d, p)	-639.6	83.8	627.0	8.3	-631.2
	X3LYP/LANL2TZ+/6-311++G(d, p)	-622.8	83.7	610.2	8.5	-614.4
	PBEPBE/6-311++G(d, p)	-647.4	81.1	635.4	9.0	-638.4
[Mn(H ₂ O) ₄ (NO ₃) ₂]	PW91PW91/6-311++G(d, p)	-652.2	81.2	635.2	9.5	-642.6
	MP2/6-311++G(d, p)	-638.4			27.1	-611.4

E_b is the stabilization energy (or binding energy), without zero-point vibration correction; ZPE is the zero-point vibrational energy, E_d^c is the dissociation energy incorporating the zero-point vibration energy correction, BSSE is the basis set superposition error, and $(E_b\text{-BSSE})$ corrects for this. Units are in kcal mol⁻¹

In a recent investigation into dichalcogen-bridged complexes of the same metals (but including Fe²⁺), the same stability order was found (with Fe²⁺ between Co²⁺ and Mn²⁺, as expected) [51]. An interesting result from that study was that MP2 gave qualitatively similar stability trends (as we find here) compared to the CCSD(T) single-point energy calculations, while the stabilities are

overestimated by DFT methods with the binding affinity in the order Cu²⁺ > Ni²⁺ > Co²⁺ > Zn²⁺ > Fe²⁺ > Mn²⁺.

Changing the basis set size to LANL2TZ+ on the metal cations and 6-311++G(d, p) on the other atoms increases the binding energy of the complexes by a few kcal mol⁻¹ while, changing the correlated functional from B3LYP to X3LYP level increases the energy of stabilization between

5 and 10 kcal mol⁻¹. This increase is presumably a result of an increase in the percentage of HF in the functional. We found a similar effect in our recent studies on Ni²⁺ and Co²⁺ with NH₃ and OH₂ ligands [1, 3].

The basis set superposition error is often taken into account and is the amount by which the energy of a transition metal cation is corrected (usually lowered) because of its complexation with the ligands. We computed this using the counterpoise procedure of Boys and Bernardi [46]. In this formalism, the metal complex under consideration is assumed to consist of seven different molecular fragments: the metal cation, four H₂O molecules and two NO₃⁻ anions. The BSSE corrected stabilization energy (E_b^{BSSE}) is the energy obtained by subtracting the BSSE energy (E^{BSSE}) from the uncorrected stabilization energy (E_b). Since we have used two types of basis sets for the complexes under study, the BSSE energy is different for the two basis sets. As can be seen from Table 2, the BSSE is almost twice as large for LANL2TZ+/6-311++G(d, p) than for 6-311++G(d, p) indicating that the ECP basis set centered on the metal ions incur a larger basis set error. The resulting BSSE corrected energies compare well with the corrected energies obtained from the 6-311++G(d, p) basis set. With PBE/PBEPBE and PW91PW91, the BSSE is somewhat larger. The BSSE is more serious using MP2 compared to a DFT-SCF method; the BSSE is as large as 27.7 kcal mol⁻¹ for the Cu²⁺ complex and 24.7 kcal mol⁻¹ for the Mn²⁺ complex. Others have also reported that MP2 has a tendency to overcorrect the binding energy [52, 53]. The binding energies are computed to increase in the order PW91PW91 < PBEPBE < X3LYP < B3LYP < MP2, indicating that the pure GGA-type DFT functionals significantly over-correct binding energies of these complexes compared to the MP2 values. Inclusion of the zero-point vibrational energy reduces the binding energies about 2%.

3.3 Effects of solvation

Generally, the poor agreement between the gas-phase-optimized structures and the solid-state structures using both DFT and MP2 methods could be due to condensed medium effects. This prompted us to re-optimize all the structures (but only at the B3LYP and X3LYP levels together with the 6-311++G(d, p) basis set) in the presence of solvent water ($\epsilon = 78.39$) and a cavity consisting of tesserae of average area of 0.3 Å² using the polarized continuum model (PCM) of Tomasi et al. [54]. We used TSNUM = 100 for the number of surface elements for each sphere, instead of the default 60, to avoid oscillatory behavior during geometry optimizations. Figure S3 of the Supporting Information shows a comparison of the structure of [Ni(H₂O)₄(NO₃)₂]²⁺, as example, determined in the gas phase and with the solvent model, as well as the solid-

state structure. The geometric agreement between the gas-phase and solvent structures is reasonable. More complete details are given in Table 1.

The most noticeable effect of solvation on the gas-phase structures is that it shortens the M–OH₂ bonds and lengthens the M–ONO₂ bonds such that the difference between the computed and the crystallographically observed bond lengths (Δ in Table 1) tends to decrease. In addition, the two intramolecular H bonds disappear.

The differences in stabilization energy ΔE between the gas-phase and solvated structures are listed in Table 3. The total energy in solution using the PCM model is the sum of the total energies of the solute, the solvent, and the cavity energy. The stabilization of the complexes is clearly evident upon solvation. In passing from Mn²⁺ to Cu²⁺ across the series, we observed a systematic decrease in the values of ΔE , and then an increase for Zn²⁺. The B3LYP mean bond lengths are marginally longer than those obtained using X3LYP, while ΔE values are marginally larger when using B3LYP.

As pointed out by a referee, it is a moot point whether optimizations carried out in water solvent are more representative of the crystalline phase than gas-phase calculations. The presence of a model for solvent certainly improves the agreement with the solid-state data. This suggests that condensed phase effects are indeed important and that the modeling should be conducted with techniques that adequately model the solid state. We are considering this and, if our enquiries yield useful results, will report on them elsewhere.

3.4 Electronic properties: NPA analysis

Charge transfer between a metal ion and its ligands is to be expected on complex formation. The charges on O atoms in the free ligands H₂O and NO₃⁻ anion, computed at the

Table 3 The stabilization energy in solution ($\Delta E = E_{\text{sol}} - E_{\text{gas}}$) of trans-[M(H₂O)₄(NO₃)₂] determined by B3LYP and X3LYP with a 6-311++G(d, p) basis set

M	Method	$E_{\text{sol}}/\text{au}^{\text{a}}$	$E_{\text{gas}}/\text{au}^{\text{a}}$	$\Delta E/\text{kcal mol}^{-1}$
Mn ²⁺	B3LYP	-2017.848175	-2017.795636	-33.0
	X3LYP	-2017.474100	-2017.422274	-32.5
Co ²⁺	B3LYP	-2249.572329	-2249.522671	-31.2
	X3LYP	-2249.190774	-2249.141198	-31.1
Ni ²⁺	B3LYP	-2375.1089119	-2375.059846	-30.8
	X3LYP	-2374.722276	-2374.674149	-30.2
Cu ²⁺	B3LYP	-2507.252598	-2507.20625	-29.1
	X3LYP	-2506.862063	-2506.815559	-29.2
Zn ²⁺	B3LYP	-2646.143488	-2646.0919	-32.4
	X3LYP	-2645.750376	-2645.698842	-32.3

^a 1 au = 627.5095 kcal mol⁻¹

X3LYP (B3LYP)/6-311++G(d, p) level, are $-0.915e$ ($-0.913e$) and $-0.562e$ ($-0.561e$), while those on the H and N atoms are $0.686e$ ($0.682e$) and $0.457e$ ($0.457e$), respectively. There is a regular and systematic redistribution of partial atomic charges among the atoms in the ligands constituting the complexes. The charges on the O atoms of NO_3^- anion involved in the dative bonding with Mn^{2+} are $-0.622e$ ($-0.620e$); with Co^{2+} , $-0.621e$ ($-0.618e$); with Ni^{2+} $-0.609e$ ($-0.606e$); with Cu^{2+} , $-0.616e$ ($-0.611e$); and with Zn^{2+} , $-0.649e$ ($-0.648e$) when computed at the X3LYP(B3LYP)/6-311++G(d, p) level. Thus, the charge on the O atom of coordinated NO_3^- decreases from the Mn^{2+} through Ni^{2+} and then increases from Ni^{2+} through to Zn^{2+} , i.e., they parallel the ionic radii [55] (and hence the polarizing power) of the ions: Mn^{2+} 0.83 Å; Co^{2+} 0.75 Å; Ni^{2+} 0.60 Å; Cu^{2+} 0.73 Å; and Zn^{2+} 0.74 Å. A similar trend is seen with the charges on the O atoms of coordinated H_2O . These range from -0.966 to $-0.968e$ in Mn; from -0.956 to -0.959 in Co; from -0.951 to $-0.955e$ in Ni; from -0.947 to -0.962 in Cu; and from -0.983 to $-0.986e$ in Zn.

Among the chosen DFT methods, the pure GGA functionals produce larger values of ΔQ than the two hybrid functionals. Nevertheless, we notice a persistent trend in the ΔQ values ($\text{Cu}^{2+} > \text{Ni}^{2+} > \text{Co}^{2+} > \text{Mn}^{2+} > \text{Zn}^{2+}$) with the 6-311++G(d, p) basis set irrespective of whether the medium is solvent or gas phase. This parallels reasonably well the electronegativity χ of the divalent cations, which can be estimated from the empirical method of Portier et al. [56], which uses the ionic radius and the charge on the ion: Cu^{2+} 1.62; Ni^{2+} 1.60; Co^{2+} 1.54; Mn^{2+} 1.44; and Zn^{2+} 1.48. Solvation decreases the magnitude of ΔQ , as expected.

As we previously remarked, the MP2 method is computationally expensive compared to the DFT functionals but it gives reliable gas-phase structural parameters that compare satisfactorily with the solid-state structures. The bond lengths are shorter while the binding energies are somewhat smaller, except for the Zn complex, compared to the DFT-predicted values. However, a discrepancy is found compared to the DFT results (with SCF density) when we performed NPA calculations at the MP2 level (with MP2 density) for the evaluation of partial atomic charges of these complexes across the series. Table 4 shows the computed charges on the metal ions in the complexes. The MP2/6-311++G(d, p) predicts the smallest value to the Ni ion ($1.691 e$) and the largest value ($1.773 e$) to the Zn ion. Thus, the ligand-to-metal charge transfer follows the pattern $\text{Ni}^{2+} > \text{Co}^{2+} > \text{Mn}^{2+} > \text{Cu}^{2+} > \text{Zn}^{2+}$, which is at odds with the electronegativity of the cations. Moreover, changing the basis set to LANL2TZ+/6-311++G(d, p) altered the ΔQ values of Ni^{2+} and Cu^{2+} in the complexes indicating that the basis set is inadequate for the prediction of charge transfer for these complexes.

Table 4 Computed NPA metal-to-ligand charge transfer ($\Delta Q/e$) values of the complexes

X3LYP		B3LYP		MP2		PBPBE		PW91PW91	
Gas 6-311++G(d, p)	Solvent 6-311++G(d, p)	Gas LANL2TZ+/ 6-311++G(d, p)	Solvent 6-311++G(d, p)	Gas LANL2TZ+/ 6-311++G(d, p)	Gas 6-311++G(d, p)				
Mn^{2+}	0.474	0.438	0.426	0.476	0.442	0.428	0.295	0.573	0.576
Co^{2+}	0.504	0.481	0.508	0.509	0.489	0.514	0.302	0.673	0.676
Ni^{2+}	0.548	0.519	0.559	0.557	0.530	0.567	0.309	0.719	0.720
Cu^{2+}	0.552	0.523	0.555	0.566	0.535	0.559	0.285	0.727	0.726
Zn^{2+}	0.331	0.317	0.269	0.335	0.320	0.265	0.227	0.391	0.390

Therefore, the MP2-derived NPA charges cannot be used for a realistic description of electronic effects in the complexes of types chosen here. The discrepancy could be a MP2 failure because of the fact that the perturbation procedure adopted in this formalism presumably performs on a wrong initial determinant compared to the DFT formalism [57, 58]. We, therefore, continue the rest of our exploration at the X3LYP/6-311++G(d, p) level of theory.

The NBO NLMO calculations identify the presence of the hydrogen-bonding interactions in these complexes irrespective whether the medium is gas or solvent. According to NBO theory, the charge transfer mechanism requires the presence of both a donor atom and an acceptor atom.

Our calculations show that the each of the lone pairs of O atoms (H-bonded) contribute to the charge transfer energy $E^{(2)}$. For instance, in case of the Zn^{2+} complex, there is a delocalization from LP(1), LP(2), and LP(3) of O atom of NO_3^- (H-bonded) \rightarrow BD*(1) O–H (of H_2O). Such delocalizations are in the range 1–6 kcal mol $^{-1}$ in the gas phase for all the complexes. Upon solvation, there is an increase in the strengths of the H bonds; the overall delocalization energies are in the range 5–15 kcal mol $^{-1}$.

3.5 Topological properties of the electron charge density: characterization of the bonding

Bader's quantum theory of atoms in molecules is useful for characterizing the electronic structure of molecules or an extended array of atoms based on the topology of the electron charge density at bond critical points [42]. According to this model, the presence of a bcp and a bond path meets the necessary conditions that two atoms are bonded to each other [42]. The values of ρ_c , where the subscript c refers specifically to the bcp, provide a measure of bond order for a series of bonds between similar atoms. We have already demonstrated the usefulness of the methodology in coordination complexes of several first row transition metals [1–3].

For a predominantly covalent (“shared”) interaction, ρ_c is usually >0.1 au [59] and the Laplacian of ρ_c , $\nabla^2 \rho_c < 0$ [59], but it may be positive for very polar bonds [60]. If the interaction is predominantly ionic (“closed shell”), the value of ρ_c is usually small ($\sim 10^{-2}$ au for a H bond and $\sim 10^{-3}$ au for a van der Waals' interaction [59]) while $\nabla^2 \rho_c > 0$. At the boundary between the two regions, i.e., at $\nabla^2 \rho_b \sim 0$, the binding is an admixture of the two.

The results of our analysis of the topology of the electron density are summarized in Table 5 for the free ligands (both in the gas phase and in solution) and in Tables 6 and 7 for the solvated complexes.

The charge density at the N–O bcp of NO_3^- is larger than that at the H–O bcp of H_2O (Table 5) as expected because the delocalization of π electron density will result in a larger accumulation of the charge density at the former bcp. The X3LYP values are slightly larger than the B3LYP values because the bond lengths computed at the former level are somewhat shorter. Values of $\nabla^2 \rho_c$ for the N–O and H–O bonds are negative (indicative of a predominantly covalent bond).

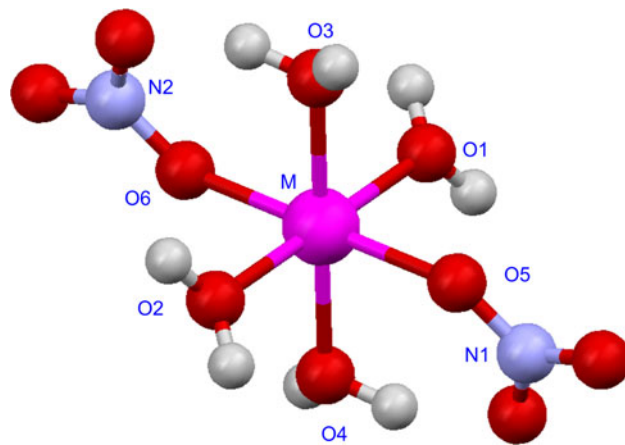
The value of ellipticity, $\varepsilon = |\lambda_1|/|\lambda_2| - 1$, for the O–H bond is near (but not exactly) zero (because of the distorting effect of the non-bonded density on O), whereas for the N–O bond in NO_3^- the value of ε is relatively large, as a consequence of the π -character of this bond [61].

The bond to the H_2O ligand that is H-bonded to coordinated nitrate is longer than that to the other H_2O ligand; the difference can be very small (0.002 Å in the Co^{2+} complex, see Table S1) to significant (0.039 Å in the Zn^{2+} complex); in the Cu^{2+} complex, compounded by a Jahn–Teller distortion, the difference is very large (0.349 Å). The M–O bond lengths themselves vary linearly with the ionic radius [55] of the divalent metal ion (Fig. 2) with the exception of the bonds in the Cu^{2+} complex because of the Jahn–Teller distortion associated with a d⁹ electron configuration. The variation of bond lengths is reflected in the values of ρ_c (a measure of the strength of the bond between the atoms [62–69]); these decrease almost linearly with the M–O bond length (Figure S4).

Table 5 The structural, zero-point energies, and topological properties of the ligands obtained from the 6-311++G(d, p) basis set

Ligand	Method	N–O and R–O/Å	ONO and HOH/deg	ZPVE/kcal mol $^{-1}$	ρ_c	λ_1	λ_2	λ_3	$\nabla^2 \rho_c$	ε	V_c	G_c	H_c
NO_3^-	B3LYP	1.2601	120.0	8.68	0.4599	-1.2060	-1.0822	1.4594	-0.8289	0.1144	-0.8633	0.3281	-0.5353
	X3LYP	1.2586	120.0	8.73	0.4616	-1.2134	-1.0878	1.4662	-0.8350	0.1154	-0.8690	0.3301	-0.5389
	X3LYP(solv)	1.2553	120.0	8.61	0.4657	-1.2293	-1.1003	1.4684	-0.8613	0.1173	-0.8815	0.3313	-0.5484
H_2O	B3LYP	0.9620	105.1	13.36	0.3664	-1.7754	-1.7312	1.0140	-2.4926	0.0255	-0.7735	0.0752	-0.6983
	X3LYP	0.9615	105.1	13.38	0.3667	-1.7842	-1.7402	1.0190	-2.0253	0.0253	-0.7765	0.0751	-0.7014
	X3LYP(solv)	0.9696	104.4	12.84	0.3562	-1.7530	-1.7145	0.9968	-2.4707	0.0224	-0.7541	0.0682	-0.6859

1 au of $\rho_c = 6.7483$ eÅ $^{-3}$, 1 au of $\nabla^2 \rho_c = 24.099$ eÅ $^{-5}$ and 1 au of G_c , V_c , and $H_c = 627.5095$ kcal mol $^{-1}$

Table 6 QTAIM properties of the metal–oxygen bonds in solvated trans-[M(H₂O)₄(NO₃)₂] complexes at the X3LYP/6-311++G(d, p) level of theory

M	Bond	ρ_c	λ_1	λ_2	λ_3	ε	$\nabla^2\rho_c$	V_c	G_c	H_c	$ V_c /G_c$	ΔQ
Mn ²⁺	Mn–O1 ^a	0.0466	-0.0614	-0.0562	0.3523	0.09253	0.2347	-0.0551	0.0569	0.0018	0.9681	0.4062
	Mn–O3	0.0520	-0.0704	-0.0656	0.3984	0.07317	0.2624	-0.0634	0.0645	0.0011	0.9827	
	Mn–O5	0.0489	-0.0636	-0.0605	0.3720	0.05124	0.2479	-0.0588	0.0604	0.0016	0.9741	
Co ²⁺	Co–O1	0.0556	-0.0761	-0.0517	0.4509	0.47195	0.3231	-0.0771	0.0790	0.0018	0.9769	0.5495
	Co–O3	0.0588	-0.0753	-0.0572	0.4598	0.31643	0.3273	-0.0808	0.0813	0.0005	0.9938	
	Co–O5	0.0528	-0.0571	-0.0487	0.4078	0.17248	0.3020	-0.0731	0.0743	0.0012	0.9835	
Ni ²⁺	Ni–O1	0.0555	-0.0537	-0.0507	0.4290	0.05917	0.3246	-0.0798	0.0805	0.0007	0.9916	0.6501
	Ni–O3	0.0613	-0.0626	-0.0592	0.4794	0.05743	0.3576	-0.0897	0.0895	-0.0001	1.0016	
	Ni–O5	0.0583	-0.0581	-0.0550	0.4527	0.05636	0.3395	-0.0844	0.0847	0.0002	0.9974	
Cu ²⁺	Cu–O1	0.0357	-0.0388	-0.0363	0.2086	0.06887	0.1335	-0.0426	0.0380	-0.0046	1.1209	0.7055
	Cu–O3	0.0735	-0.0931	-0.0895	0.5829	0.04022	0.4002	-0.1081	0.1041	-0.0040	1.0386	
	Cu–O5	0.0670	-0.0819	-0.0790	0.5174	0.03671	0.3565	-0.0958	0.0924	-0.0033	1.0360	
Zn ²⁺	Zn–O1	0.0540	-0.0684	-0.0642	0.3681	0.06542	0.2355	-0.0725	0.0657	-0.0068	1.1039	0.5816
	Zn–O3	0.0600	-0.0778	-0.0742	0.4202	0.04852	0.2682	-0.0823	0.0747	-0.0076	1.1023	
	Zn–O5	0.0538	-0.0665	-0.0638	0.3650	0.04232	0.2347	-0.0726	0.0657	-0.0070	1.1063	

The mean values of charge density (ρ_c) and its Laplacian ($\nabla^2\rho_c$) at the M–O bcp's are in au (1 au of $\rho_c = 6.7483 \text{ e}^{-3} \text{ \AA}^{-3}$, and 1 au of $\nabla^2\rho_c = 24.099 \text{ e}^{-5} \text{ \AA}^{-5}$). The energy density values at bcp's are in au (1 au = 627.5095 kcal mol⁻¹)

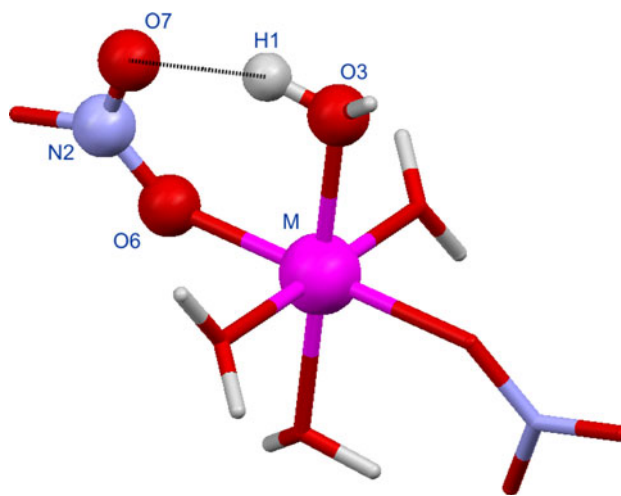
Because of the C_i symmetry of these complexes, the properties of each M–O bond are identical to the bond trans to it. Only the three unique M–O bonds are listed

Coordination of NO₃⁻ to a metal causes an elongation of the O–N bond (from 1.255 Å in free NO₃⁻ to 1.279, 1.278, 1.283, 1.289, and 1.281 Å, respectively, in the Mn²⁺, Co²⁺, Cu²⁺, Ni²⁺, and Zn²⁺ complexes). Accompanying this elongation is a decrease in ρ_c . For example, in the Cu²⁺ complex, ρ_c is 0.4386 au compared to 0.4657 in free NO₃⁻. This is undoubtedly a consequence of the polarization effect of the metal cation on the electron density of the ligand.

The values of $\nabla^2\rho_c$ (Table 6) are positive both for all three types of M–O bonds, indicative of the predominantly ionic nature of the bonding between the divalent metal cations and the hard O donors of the ligands [70].

The ellipticity values for all M–O bonds are <0.1 except for the Co²⁺ complex where they are unexpectedly large suggesting there is some multiple bond character to the metal–ligand bonds. Why this should be the case is unclear and probably merits further investigation.

Hydrogen bonding between a coordinated water molecule and one of the O atoms of coordinated NO₃⁻ occurs in all complexes. As pointed out earlier, this leads to an elongation and weakening of the metal–OH₂ bond. From the relationship put forward by Espinosa et al. [71], $E_{hb} = \frac{1}{2}V_c$, these H bonds are estimated to have a strength of some 9–11 kcal mol⁻¹ in our solvated structure models (and between 4 and 9 kcal mol⁻¹ in the gas-phase models).

Table 7 The ring critical points (rcp's) and H bonds in solvated trans-[M(H₂O)₄(NO₃)₂] complexes at the X3LYP/6-311++G(d, p) level of theory

Rcp's and H bonds in complexes ^a	ρ_c	λ_1	λ_2	λ_3	$\nabla^2 \rho_c$	V_c	G_c	H_c	$E_{hb}/\text{kcal mol}^{-1}$
Mn²⁺									
(3, +1) rcp Mn–O6–N2–O7–H1–O3	0.0099	−0.0074	0.0141	0.0329	0.0396	−0.0082	0.0090	0.0004	
(3, −1) bcp O7–H1	0.0340	−0.0527	−0.0498	0.2199	0.1174	−0.0288	0.0291	0.0001	−9.1
Co²⁺									
(3, +1) rcp Co–O6–N2–O7–H1–O3	0.0110	−0.0082	0.0187	0.0332	0.0437	−0.0092	0.0101	0.0004	
(3, −1) bcp O7–H1	0.0366	−0.0582	−0.0552	0.2371	0.1238	−0.0320	0.0314	−0.0003	−10.0
Ni²⁺									
(3, +1) rcp Ni–O6–N2–O7–H1–O3	0.0109	−0.0075	0.0232	0.0277	0.0434	−0.0091	0.0100	0.0004	
(3, −1) bcp O7–H1	0.0318	−0.0473	−0.0448	0.2050	0.1129	−0.0265	0.0273	0.0004	−8.3
Cu²⁺									
(3, +1) rcp Cu–O6–N2–O7–H1–O3	0.0117	−0.0094	0.0228	0.0330	0.0464	−0.0099	0.0107	0.0004	
(3, −1) bcp O7–H1	0.0386	−0.0624	−0.0600	0.2515	0.1291	−0.0345	0.0334	−0.0006	−10.8
Zn²⁺									
(3, +1) rcp Cu–O6–N2–O7–H1–O3	0.0103	−0.0083	0.0175	0.0305	0.0397	−0.0083	0.0091	0.0004	
(3, −1) bcp O7–H1	0.0369	−0.0588	−0.0565	0.2400	0.1247	−0.0324	0.0318	−0.0003	−10.2

H bond strengths are from the relationship $E_{hb} = \frac{1}{2}V_c$. 1 au of $\rho_c = 6.7483 \text{ e}\text{\AA}^{-3}$, and 1 au of G_c , V_c , and $H_c = 627.5095 \text{ kcal mol}^{-1}$

^a Because of the C_i symmetry with the metal as inversion center, there is an equivalent rcp and H bond across the molecule

Their presence is confirmed by the appearance of a (3, +1) ring critical point as the M–O6–N2–O7···H1–O3 bond paths form an annular structure (Table 7).

There is an inverse correlation between the H1–O3 bond length and the O7···H1 distance (Figure S7A); as the hydrogen bond increases in strength ($\text{Cu}^{2+} > \text{Zn}^{2+} > \text{Co}^{2+} > \text{Mn}^{2+} > \text{Ni}^{2+}$) and the distance between O7 and H1 decreases, the H1–O7 bond weakens and elongates. The increasing strength of the hydrogen bond causes a decrease in the value of H_c at the bcp (Figure S7B), such that for Zn^{2+} , Co^{2+} and Cu^{2+} , $H_c < 0$ indicating a significant covalency in the hydrogen bond. However, there is never a complete transfer of the proton from H_2O to NO_3^- .

The sign of the Laplacian of the charge density, together with the values of ρ_c at a bcp, may not always be sufficient to characterize the nature of an interaction present in a chemical system. Cremer and Kraka [72, 73], therefore, used the sign and magnitude of the total energy density H_c as an indicator of the nature of a bonded interaction. The total energy density, which is the sum of the local potential and kinetic energy densities, $H_c = V_c + G_c$, is used to distinguish such interactions: $H_c < 0$ for covalent interactions where V_c dominates, and $H_c > 0$ for ionic interactions since G_c dominates in such situations. The negative values of H_c confirm the covalent nature of the N–O and H–O bonds.

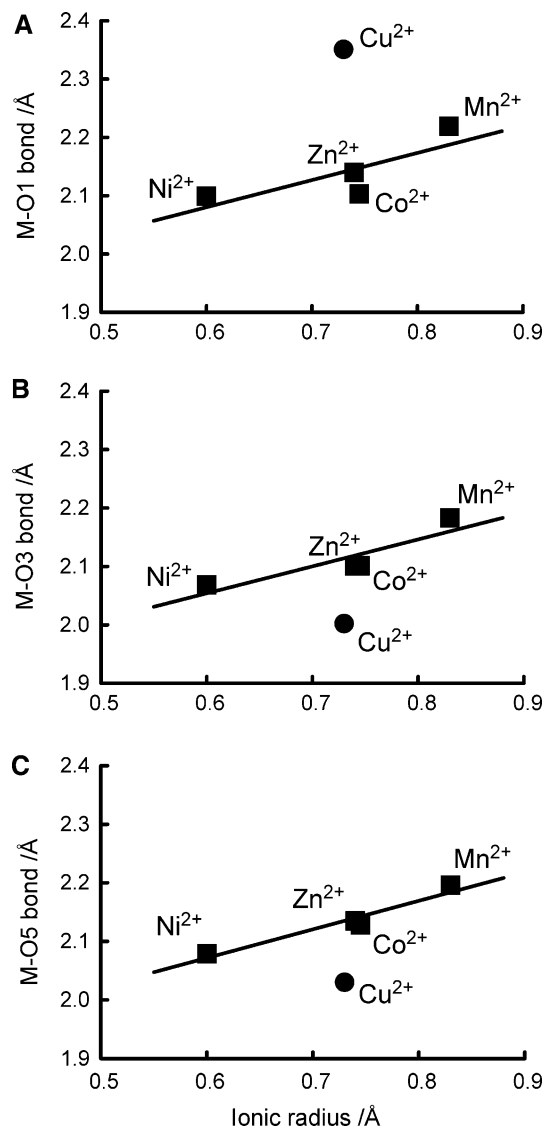


Fig. 2 Dependence of the metal–oxygen bond lengths in $[M(H_2O)_4(NO_3)_2]$ complexes as a function of the Shannon ionic radius of the metal ion (excluding values for Cu^{2+}). Refer to Table 6 for atom numbering

Several groups have suggested using the ratio $|V_c|/G_c$ to characterize a bond [74, 75]. Interactions with $|V_c|/G_c < 1$ are characteristics of ionic interactions; those with $|V_c|/G_c > 2$ are typically covalent interactions, while interactions with $1 < |V_c|/G_c < 2$ have intermediate character. On this basis (Table 6), the bonding between the ligands and Mn^{2+} , Co^{2+} and Ni^{2+} is ionic, whereas that with Cu^{2+} and Zn^{2+} has partial covalent character. This is confirmed by the values of H_c since ionic bonds have $H_c > 0$ and close to zero [70], while for interactions with some covalent character, $H_c < 0$ [60, 72, 75, 76]. The average value of $|V_c|/G_c$ increases monotonically with atomic number (Figure S5). Surprisingly, we could find no strong correlation between this parameter and either the absolute hardness of the metal

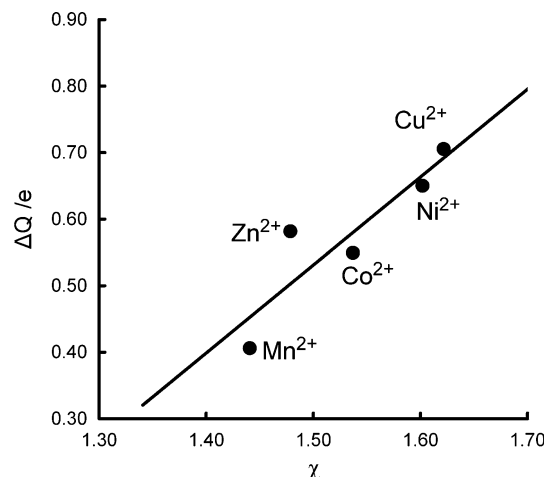


Fig. 3 Dependence of the Bader charge transferred to the divalent metal ion (ΔQ_{Bader}) and the empirical electronegativity (χ) as defined by Portier et al. [56], in $[M(H_2O)_4(NO_3)_2]$ complexes ($r^2 = 0.81$)

ion as defined by Parr and Pearson [77], or with the electronegativity χ of the cation, estimated using the empirical correlation of Portier et al. [56], which uses the ionic radius and the charge on the ion, together with an element-specific empirical factor to determine χ nor a combination of both factors (Figure S6). The Portier electronegativities, however, correlate reasonable well with the charge transferred to the metal, ΔQ_{Bader} (Fig. 3).

4 Summary

We have energy-minimized the structures of $[M(H_2O)_4(NO_3)_2]$ ($M = Mn^{2+}$, Co^{2+} , Ni^{2+} , Cu^{2+} , Zn^{2+}) under C_i symmetry using two correlated methods, B3LYP and X3LYP, together with two basis sets, 6-311++G(d, p) and LANL2TZ +/6-311++G(d, p), to compare the predicted structures with available crystallographic data, and that to determine their stabilities. We found that the NO_3^- anions bound to the metal in a monodentate manner, and that the $M-OH_2$ and $M-ONO_2$ bond lengths deviate somewhat from the crystallographically observed bond lengths. In particular, DFT methods over-estimate the ligating ability of NO_3^- and metal– ONO_2 bonds are invariably too short, at the expense of metal– OH_2 bonds which are, conversely, too long.

Gas-phase calculations were also extended to the PBEPBE, PW91PW91 and MP2 levels in conjunction with the 6-311++G(d, p) basis set to explore the feasibility of reproducing the exact crystallographic structures. The binding energies were found to be somewhat larger while again the overall geometry of the complexes did not change markedly.

The stabilities of the complexes predicted depended on the method used and were in the order PW91PW91 < PBEPBE < X3LYP < B3LYP < MP2; this indicates that the DFT functionals, especially the pure GGA functionals, overestimate largely the stabilization energies of the complexes compared to MP2. The metal–ligand binding energies follow the trend $\text{Cu}^{2+} > \text{Ni}^{2+} > \text{Zn}^{2+} > \text{Co}^{2+} > \text{Mn}^{2+}$ across the series examined irrespective of the correlated methods or basis sets used. The BSSE affects are more significant at the MP2 level than at the DFT-SCF level of theory.

Incorporating a solvent model into the calculations improves matters somewhat. The calculations show the presence of four hydrogen bonds in the gas-phase structures; in the solvent calculations, two of these hydrogen bonds disappear. Placing an ECP basis on the metal and using a 6-311++G(d, p) basis set on the main group elements increase the binding energies of the complexes compared to that found using 6-311++G(d, p), a full-core basis set. While the geometry does not change significantly, energy differences of up to 20 kcal mol⁻¹ were found.

An examination of the NPA charges on the atoms showed that there is charge transfer from the ligands to the divalent metal ions. The charges determined using MP2 or those obtained with the LANL2TZ+/6-311++G(d, p) appear to be unreliable. The DFT methods predict that the charge transferred to the metal ions decrease in the order $\text{Cu}^{2+} > \text{Ni}^{2+} > \text{Co}^{2+} > \text{Mn}^{2+} > \text{Zn}^{2+}$, in reasonable agreement with the electronegativity of the cations in the gas phase. The B3LYP and X3LYP functionals swap the order for Ni and Cu when changing the basis set from 6-311++G(d, p) to LANL2TZ+/6-311++G(d, p), indicating that the latter basis set is insufficient for describing the NPA charges of the metal cations in these complexes. The order of charge transfer determined by the QTAIM theory of Bader on the solvated structure is in line with the stability of the complexes in the series.

The bonding characteristics of the complexes were examined using QTAIM. Several indicators suggest that the M–O bond is predominantly ionic although the degree of covalency increases as the atomic number of the metal ion increases. The charge transferred to the metal, ΔQ^{Bader} , ions correlate reasonably with the electronegativity of the metal.

Acknowledgments PRV acknowledges the Japan Society for the Promotion of Science (JSPS) for the award of a Postdoctoral Fellowship and financial support received for conducting research at the Department of Chemistry of Okayama University, Okayama, Japan. PRV gratefully acknowledges Professor K. Kawaguchi for his kind support during this work and thanks the Osaka University computer center for providing supercomputing facilities. HMM thanks the Department of Science and Technology and the National Research

Foundation, Pretoria, for funding through the South African Research Chairs Initiative.

References

- Varadwaj PR, Cukrowski I, Marques HM (2008) *J Phys Chem A* 112:10657
- Varadwaj PR, Cukrowski I, Marques HM (2009) *J Mol Str (Theochem)* 902:21
- Varadwaj PR, Marques HM (2010) *Phys Chem Chem Phys* 12:2126
- Barnett SA, Blake AJ, Champness NR, Wilson C (2005) *Dalton Trans* 3852
- Pelizzi C, Pelizzi G, Tarasconi P (1985) *J Organomet Chem* 281:403
- Beauchamp DA, Loeb SJ (2002) *Chem Eur J* 8:5084
- Barnett SA, Blake AJ, Champness NR, Wilson C (2002) *J Supramol Chem* 2:17
- Oomens J, Myers L, Dain R, Leavitt C, Pham V, Gresham G, Groenewold G, Van Stipdonk M (2008) *Int J Mass Spec* 273:24
- Brandt SA, Socolsky C, Altabef AB (2009) *Z Anorg Allg Chem* 635:582
- Morris DFC, MacCarthy JD, Newton RJ (1978) *Electrochim Acta* 23:1383
- Aruga R (1975) *J Chem Soc Dalton Trans* 2534
- Hutchinson MH, Higginson CE (1973) *J Chem Soc Dalton Trans* 1247
- Martell AE, Motekaites RJ (1992) Determination and use of stability constants, 2nd edn. Wiley-VCH, New York
- Ohtaki H, Radnai T (1993) *Chem Rev* 93:1157
- Ramesh SG, Re S, Hynes JT (2008) *J Phys Chem A* 112:3391
- Pathak AK, Mukherjee T, Maity DK (2008) *J Phys Chem A* 112:3399
- Goebbert DJ, Garand E, Wende T, Bergmann R, Meijer G, Asmis KR, Neumark DM (2009) *J Phys Chem A* 113:7584
- Popov D, Herak R, Prelesnik B, Ribár B (1973) *Zeit Krist* 137:280
- Popov D, Herak R, Radulovic N, Ribár B (1975) *Zeit Krist* 142:347
- Ribár B, Milinski N, Herak R, Krstanovic I, Djuric S (1976) *Zeit Krist* 144:133
- Blake AJ, Brett MT, Champness NR, Khlobystov AN, Long D-L, Wilson C, Schroder M (2001) *J Chem Soc Chem Commun* 2258
- Siegler MA, Parkin S, Selegue JP, Brock CP (2008) *Acta Crystlogr Sect B* 64:725
- Bigoli F, Braibanti A, Tiripicchio A, Tiripicchio Camellini M (1971) *Acta Cryst Sec B* 27:1427
- Ribár B, Milinski N (1975) *Zeit Krist* 142:303
- Gallezot P, Weigel D, Pretté M (1967) *Acta Cryst* 22:699
- Morosin B, Haseda T (1979) *Acta Cryst Sec B* 35:2856
- Ribár B, Milinski N (1977) *Zeit Krist* 144:126
- Petrovic D, Ribár B (1975) *Acta Cryst Sec B* 31:1795
- Ribár B, Nowacki W, Sljukic M, Scavnica S, Gabela F (1969) *Zeit Krist* 129:305
- Ribár B, Nowacki W, Sljukic M, Gabela F, Matkovic B (1970) *Zeit Krist* 131:175
- Jacquemin D, Perpete EA, Ciofini I, Adamo C (2005) *Chem Phys Lett* 405:376
- Xu X, Goddard WA (2004) *Proc Natl Acad Sci USA* 101:2673
- Xu X, Goddard WA (2004) *J Phys Chem A* 108:2305
- Xu X, Zhang Q, Muller RP, Goddard WA (2005) *J Chem Phys* 122:14105
- Becke AD (1993) *J Chem Phys* 98:5648

36. Stephens PJ, Devlin JF, Chabalowski CF, Frisch MJ (1994) *J Phys Chem* 98:11623
37. Perdew JP, Burke K, Ernzerhof M (1996) *Phys Rev Lett* 77:3865
38. Burke K, Perdew JP, Wang Y (1997) In: Dobson JF, Vignale G, Das MP (eds) *Electronic density functional theory: recent progress and new directions*. Plenum Press, New York, p 81
39. Curtiss LA, Raghavachari K, Pople JA (1993) *J Chem Phys* 98:1293
40. Mennucci B, Tomasi J (1997) *J Chem Phys* 106:5151
41. Cossi M, Barone V, Mennucci B, Tomasi J (1998) *Chem Phys Lett* 286:253
42. Bader RF (1990) *Atoms in molecules: a quantum theory*. Oxford University Press, Oxford
43. Frisch MJ, Trucks GW, Schlegel HB, Scuseria GE, Robb MA, Cheeseman JR, Montgomery JJA, Vreven T, Kudin KN, Burant JC, Millam JM, Iyengar SS, Tomasi J, Barone V, Mennucci B, Cossi M, Scalmani G, Rega N, Petersson GA, Nakatsuji H, Hada M, Ehara M, Toyota K, Fukuda R, Hasegawa J, Ishida M, Nakajima T, Honda Y, Kitao O, Nakai H, Klene M, Li X, Knox JE, Hratchian HP, Cross JB, Adamo C, Jaramillo J, Gomperts R, Stratmann RE, Yazyev O, Austin AJ, Cammi R, Pomelli C, Ochterski JW, Ayala PY, Morokuma K, Voth GA, Salvador P, Dannenberg JJ, Zakrzewski VG, Dapprich S, Daniels AD, Strain MC, Farkas O, Malick DK, Rabuck AD, Raghavachari K, Foresman JB, Ortiz JV, Cui Q, Baboul AG, Clifford S, Cioslowski J, Stefanov BB, Liu G, Liashenko A, Piskorz P, Komaromi I, Martin RL, Fox DJ, Keith T, Al-Laham MA, Peng CY, Nanayakkara A, Challacombe M, Gill PMW, Johnson B, Chen W, Wong MW, Gonzalez C, Pople JA (2004) Gaussian 03, 2003. Gaussian Inc., Pittsburgh
44. Dennington R, Keith T, Millam J (2007) GaussView, 4.1. Semichem, Inc., Shawnee Mission
45. Roy LE, Hay PJ, Martin RL (2008) *J Chem Theory Comput* 4:1029
46. Boys SF, Bernardi F (1970) *Mol Phys* 19:553
47. Reed AE, Wienhold F, Curtiss LA, Pochatko DJ (1986) *J Chem Phys* 84:5687
48. Weinhold F (1998) In: Schleyer PvR, Allinger NL, Clark T, Gasteiger J, Kollman PA, Schaefer HF, Schreiner PR (eds) *Encyclopedia of computational chemistry*, vol 3. Wiley, Chichester, p 1792
49. Glendening EE, Reed AE, Carpenter JE, Weinhold F (2004) NBO (Natural Bond Orbital), 3.0, as implemented in GAUSSIAN 03, Gaussian Inc., Pittsburgh
50. Keith TA (2008) AIMAll, 08.05.04, <http://aim.tkgristmill.com>
51. Jeanvoine Y, Spezia R (2009) *J Phys Chem A* 113:7878
52. Nicolaides CA, Simandiras ED (1992) *Chem Phys Lett* 196:213
53. Tan X-J, Zhu W-L, Cui M, Luo X-M, Gu J-D, Silman I, Sussman JL, Jiang H-L, Ji R-Y, Chen K-X (2001) *Chem Phys Lett* 349:113
54. Miertus S, Scrocco E, Tomasi J (1981) *Chem Phys* 55:117
55. Shannon RD (1976) *Acta Cryst A* 32:751
56. Portier J, Campert G, Etourneau J, Tanguy B (1994) *J Alloys Compds* 209:285
57. Luna A, Alcamí M, Mó O, Yáñez M (2000) *Chem Phys Lett* 320:129
58. Lynch BJ, Truhlar DG (2002) *Chem Phys Lett* 361:251
59. Bader RFW, Essén H (1984) *J Chem Phys* 80:1943
60. Bobrov MF, Popova GV, Tsirelson VG (2006) *Russ J Phys Chem* 80:584
61. Bader RFW, Slee TS, Cremer D, Kraka E (1983) *J Am Chem Soc* 105:5061
62. Howard ST, Krygowski TM (1997) *Can J Chem* 75:1174
63. O'Brien SE, Popelier PL (1999) *Can J Chem* 77:28
64. Bader RFW, Matta CF, Cortés-Guzmán F (2004) *Organometallics* 23:6253
65. Vidal I, Melchor S, Alkorta I, Elguero J, Sundberg MR, Dobado JA (2006) *Organometallics* 25:5638
66. González L, Mó O, Yáñez M, Elguero J (1996) *J Mol Str* 371:1
67. Espinosa E, Souhassou M, Lachebar H, Lecomte C (1999) *Acta Cryst B* 55:563
68. Grabowski SJ (2000) *J Phys Chem A* 105:5551
69. Sobczyk L, Grabowski SJ, Krygowski TM (2005) *Chem Rev* 105:3513
70. Bone RGA, Bader RFW (1996) *J Phys Chem* 100:10892
71. Espinosa E, Molins E, Lecomte C (1998) *Chem Phys Lett* 285:170
72. Cremer D, Kraka E (1984) *Angew Chem Int Ed Engl* 23:627
73. Cremer D, Kraka E (1984) *Croat Chem Acta* 57:1259
74. Jenkins S, Morrison I (2000) *Chem Phys Lett* 317:97
75. Espinosa E, Alkorta I, Elguero J, Molins E (2002) *J Chem Phys* 117:5529
76. Macchi P, Sironi A (2003) *Coord Chem Rev* 238–239:383
77. Parr RG, Pearson RG (1983) *J Am Chem Soc* 105:7512
78. Ribár B, Herak R, Prelesník B, Krstanović I, Milinski N (1976) *Zbor Rad Prirodno-Matemat Fakul Ser biolog*, Univ Novi Sad 5:65